Chapter 4: Studies of the Binding Site of the Mouse Muscle Nicotinic Acetylcholine Receptor[1]

4.1. Introduction

This chapter describes initial studies of the prototypical nicotinic acetylcholine receptor (nAChR), the mouse muscle nAChR. These studies were performed several years ago, and since then many advances and experiments have obtained a much more thorough understanding of the structure and function of the nAChR. A current description of these receptors is outlined along with the reasoning behind our studies of this receptor. Additionally, we incorporated computational models of the nAChR to enhance our understanding of the functional studies we performed on the receptor. In addition, background information regarding previous computational models of the receptor will be provided. There will be a discussion of how these contribute to our understanding of these ligand-gated ion channels.

4.1.1. The Nicotinic Acetylcholine Receptor

The nAChR is a ligand-gated ion channel in the Cys-loop family of ion channels. The Cys-loop family also encompases the serotonin receptors, glycine, and γ-aminobutyric acid (GABA) receptors (*1-4*). The nAChR is the prototypical Cys-loop receptor, and it is active in both the central nervous system and at the neuromuscular junction. This receptor is the target of acetylcholine, but also responds to nicotine (Nic) and many pharmaceuticals aimed at memory enhancement and Parkinson's disease (*5*). The nAChR became the prototype for ion channel studies in part due to its natural abundance in the *Torpedo* ray *electroplax* (where the receptors provide the ray's electrical shock), which allowed for the first cloning in 1982 (*6-8*). Further biochemical studies by Unwin have produced cryo-electron micrograph (cryo-EM) images of the full-length receptor (*9*).

---

[1]Reproduced in part with permission from Cashin, A.L., Torrice, M.M., McMenimen, K.A., Lesater, H.A., Dougherty, D.A. *Biochemistry* **2007**, *46*, 630–639. Copyright 2007 American Chemical Society

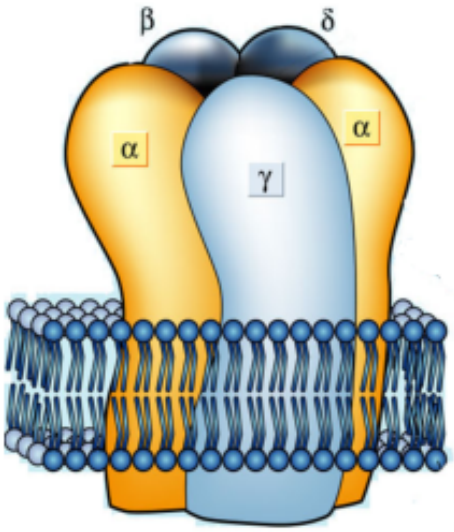

Figure 4.1 Pentameric architecture of the muscle-type nAChR with α, β, δ, α, and γ subunit arrangement.

The Cys-loop receptors all have a cylindrical, pentameric assembly and are sometimes referred to as the pentameric LGICs (Figure 4.1). The five subunits (approximately 400 amino acids in size) are pseudosymmetrically arranged around the ion-conducting pore (*10*). There are several different subunits- α, β, δ, γ, and ε- that assemble in different configurations depending on the type of α subunit present. The α subunit is required for assembly and to date there are 10 types of α subunits (α1-α10); similarly, there are four types of β (β1-4). The nAChRs found at the neuromuscular junction are referred to as the muscle-type receptor and are composed of two α1 subunits, and one β1, δ, and γ subunits. The neuronal nAChRs are composed of different combinations of α and β subunits; for example, several common neuronal nicotinic receptors are the homopentameric α7 receptors and the α4β2 receptors, which demonstrate the diversity of these receptors (*4*). Topology is conserved for all subunit types, with each containing an extracellular, N-terminal ligand-binding domain (LBD) followed by four transmembrane spanning helices (TM1-4), and a short extracellular C-terminus. Structural analysis of a homologous protein, acetylcholine binding protein (AChBP), has provided much of the structural analysis of the LBD and will be discussed below (*11*). The LBD also contains the conserved Cys-loop, for which these receptors are named (Figure 4.2). Although the arrangement of the transmembrane domains

around the pore are not conclusively determined, a lot of biochemical evidence suggests that TM2 is the pore-lining helix and TM4 is aligned closest to the membrane (Figure 4.2).

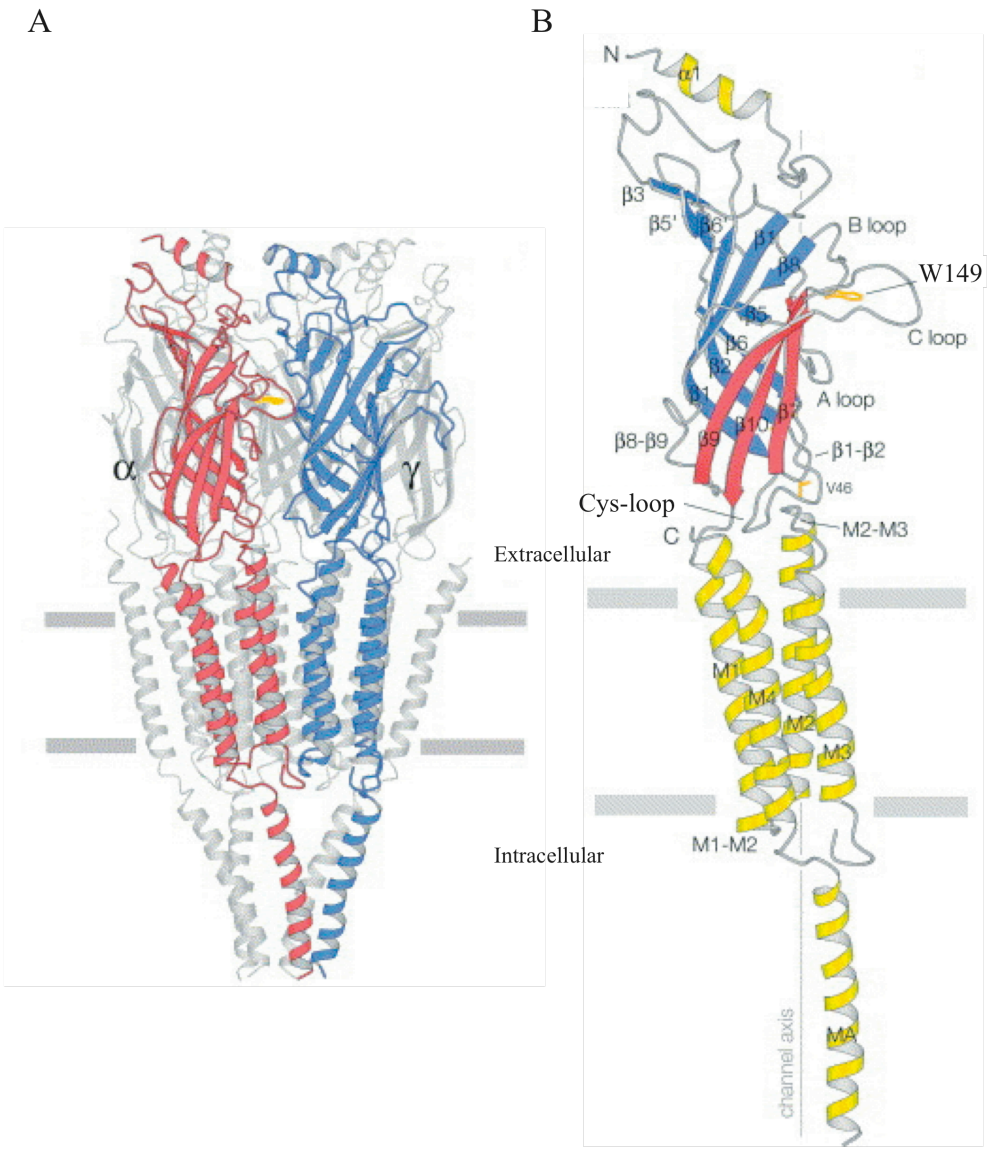

Figure 4.2 A) Structural topology of the muscle-type nAChR. B) Subunit topology of nAChR with the Cys-loop in the extracellular domain and the four TM helices, adapted from reference (*12*).

All of the experiments described were performed on the muscle-type receptor and will be the focus of the discussion. The early studies of the nAChR using unnatural

amino acids were preceded by many biochemical studies of the muscle-type receptor. These biochemical studies identified key residues likely to contribute to the ligand-binding sites in the receptor. The muscle-type receptor has two ligand-binding sites, which are located at the α/γ and α/δ subunit interfaces (*4, 13, 14*). Near the agonist binding site is a conserved disulfide bond (Cys192-Cys193, mouse muscle numbering), which was discovered by Karlin and co-workers (*15*). Several conserved loops are present in the extracellular domain and contribute to the agonist-binding site. The primary face of the binding site is located on the α-subunits and presents residues from loops A, B, and C (Figure 3). The complementary binding face is located on the δ/γ subunit and contributes loops D, and possibly E and F, to the binding site (Figure 4.2) (*16*).

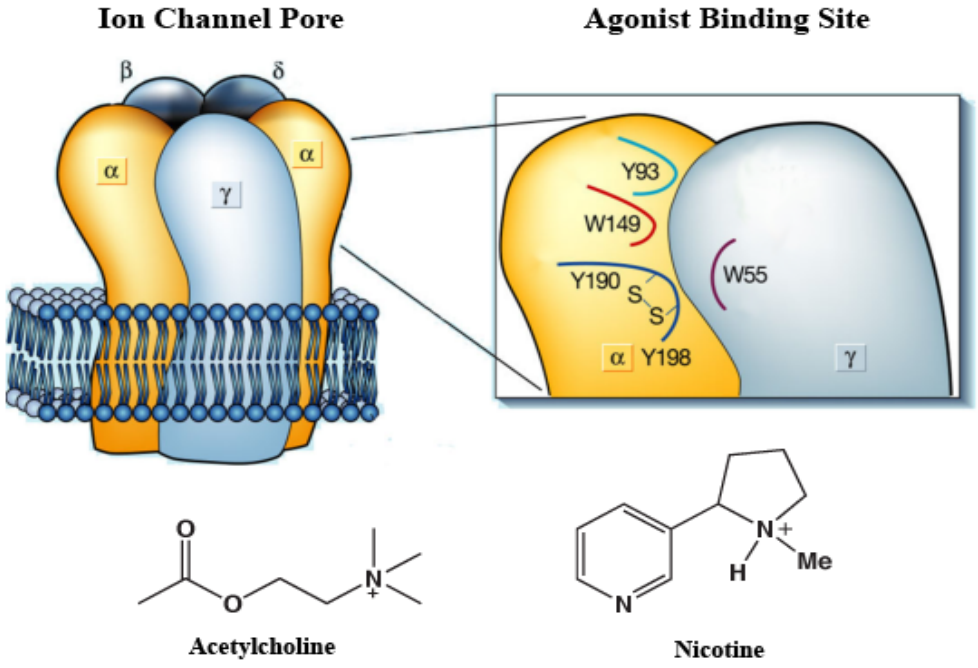

Figure 4.3 The agonist binding site is primarily comprised from α-subunit residues in loops A, B, and C. The γ-subunit contributes to the complementary face and the ligands, acetylcholine and nicotine, bind to this site.

4.1.2. Acetylcholine Binding to the nAChR

Pioneering work by Changeux using photoaffinity labeling and radio-ligand binding

studies identified many aromatic residues near the agonist binding site (*17-19*). This plethora of aromatic residues suggested that a cation-π interaction between the aromatic residues and the quaternary ammonium group of acetylcholine (ACh) may be contributing to ligand binding. We have previously demonstrated the cation-π interaction is primarily electrostatic and involves a cation binding to the electron-rich face of an aromatic ring (*20*). All of the tyrosine (Tyr) and tryptophan (Trp) residues in the binding site were evaluated for a cation-π interaction, however only Trp149 in loop B of the α subunit (Figure 4.3) was involved in the interaction with acetylcholine, as demonstrated by Zhong *et. al (21)*. Incorporation of the fluorinated tryptophan series (introduced in Chapter 2) resulted in increasing EC_{50} shifts for ACh (Figure 4.4). These studies established that Trp 149 in the "aromatic box" contributes to ligand binding through a cation-π interaction.

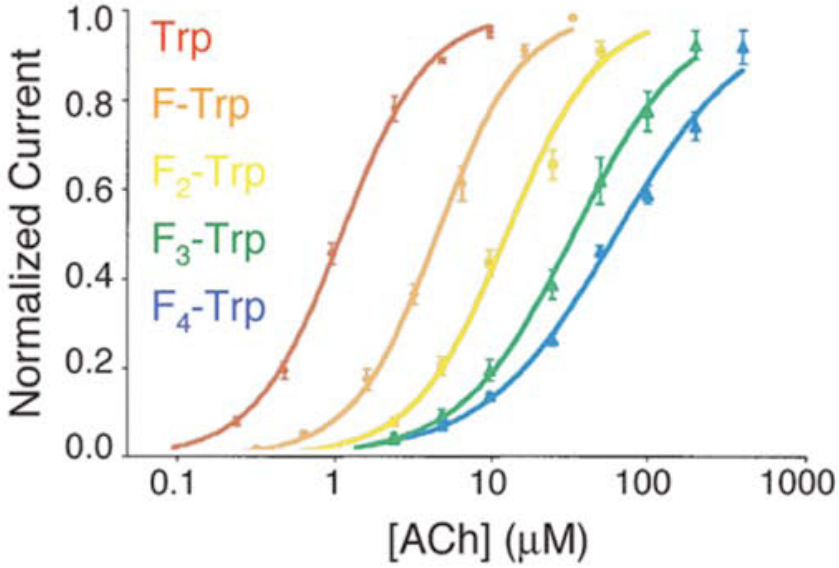

Figure 4.4 EC_{50} shifts for ACh at the mouse muscle nAChR with F_n-Trp incorporation at Trp149.

Further evidence for the aromatic box, along with more detail about the structure of the ligand binding domain of nAChRs, was established due to crystallography on the acetylcholine binding protein (AChBP), which is homologous to the extracellular ligand binding domain of nAChRs (*11, 22*). AChBP is a soluble, homopentameric protein found in snail glial cells and is 20-26% identical in sequence to nAChR LBDs and most similar

to the homomeric α7 receptor (*11, 22*). Crystal structures of AChBP, complexed with different ligands, demonstrated the presence of the "aromatic box" containing five aromatic amino acids that form a cavity where the cationic ligand binds (Figure 4.5).

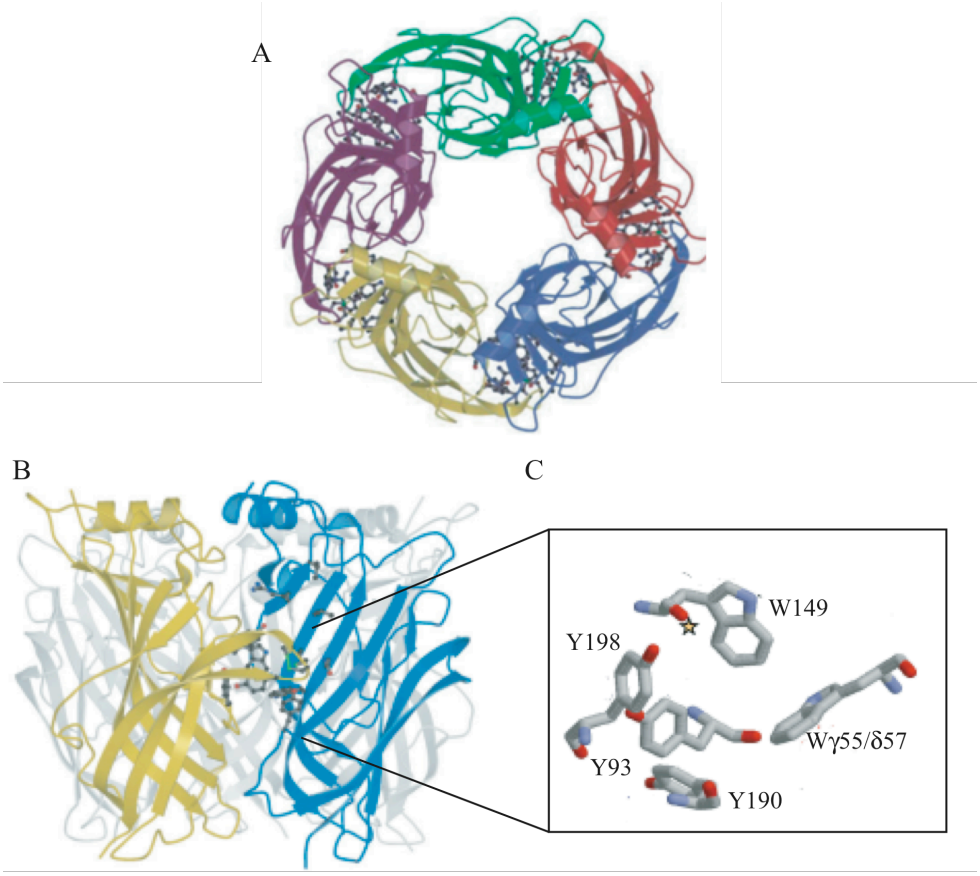

Figure 4.5. A) Pentameric structure of AChBP. B) Agonist binding site in AChBP. C) The aromatic box residues that create the binding pocket in AChBP, adapted from reference (*23*).

Currently, there are no crystal structures of any nAChRs. Therefore it is important that when we use AChBP as a guide for designing experiments, it serves as a model for the receptor with the caveat that it is *only* a model and not necessarily an accurate representation of the true receptor. The loops previously identified in biochemical experiments that contribute to the agonist binding site overlap well with those in the AChBP structure (*22, 23*). Additionally, in the original AChBP crystal structures, a molecule of HEPES, a cationic buffer, was positioned in the agonist binding

site cavity where the cationic portion of the molecule was in close proximity with AChBP Trp 143 (homologous to Trp 149 in mouse muscle) (*22, 23*).

4.1.3. Nicotine Binding to the nAChR and Ligand Discrimination

The initial studies confirming the presence of a cation-π interaction between ACh and the muscle nAChR were intriguing and led us to pursue the presence of additional cation-π interactions involved in recognition of other nAChR agonists. Due to the cationic nature of (-)-nicotine (Figure 4.3), it was hypothesized to bind the nicotinic acetylcholine receptor in a similar manner to ACh (i.e., via a cation-π interaction) (*24*). Cohen *et al.,* used photoaffinity labeled nicotine analogs to investigate how nicotine binds to the muscle nAChR. Interestingly, these experiments identified the same aromatic residues involved in ACh binding, suggesting that ACh and nicotine utilize the same residues for agonist binding (*25*). However, incorporation of the F_n-Trp derivatives at Trp149 of the muscle receptor did not produce a similar trend in the fluorination plot compared to ACh binding, which suggested that nicotine does not utilize a cation-π interaction (*26*). The other residues within the agonist binding box were also tested for the presence of a cation-π interaction, but did not demonstrate the interaction (Figure 4.6).

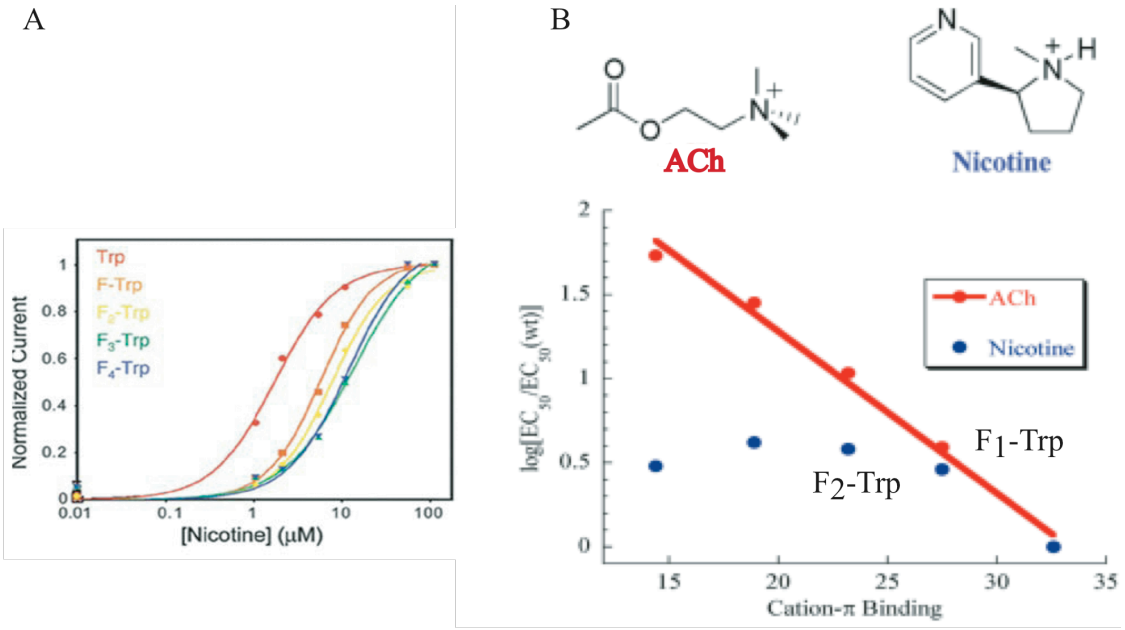

Figure 4.6. A) EC_{50} shifts for F_n-Trp incorporation at α149 in mouse muscle nAChR. No shift is observed after F_1-Trp incorporation. B) Fluorination plot for ACh and nicotine binding to muscle nAChR. A linear relationship is observed for ACh but not for nicotine, indicating the absence of a cation-π interaction.

Previously, all cationic agonists were believed to interact with the receptor in a similar way. However, these results separated the ligands into two classes, the "cholinergic" agonists such as ACh, and the "nicotinic" agonists that bind similarly to nicotine. One intriguing feature of the nicotine fluorination plot is that it begins with a shift in EC_{50}, like the cholinergic agonists, and then changes its path. These plots correspond to a Hammett-like plot and the "break" in the curve (two different slopes) suggests that nicotine binds using one mechanism and then fluorination of α149 could result in a change in the binding mechanism. On the other hand, it is possible that nicotine never interacts with the binding site through a cation-π interaction at the muscle nAChR. Another noticeable difference between ACh and nicotine binding to the muscle nAChR is that nicotine is approximately 100-fold less potent than ACh, indicating that other interactions are involved in the binding and/or gating mechanisms for Nic. This establishes that the receptor is able to discriminate between different types of ligands. Previous modeling studies suggested that nicotine makes a hydrogen bond between the N^+-**H** to the backbone carbonyl of αTrp149 (*27, 28*). Sixma and co-workers

simultaneously published a crystal structure of AChBP with nicotine bound, confirming the presence of the hydrogen bond between nicotine and the backbone carbonyl of αTrp149 (*29*). Although both ACh and nicotine agonists bind to the same site in the receptor, they utilize different non-covalent interactions to do so.

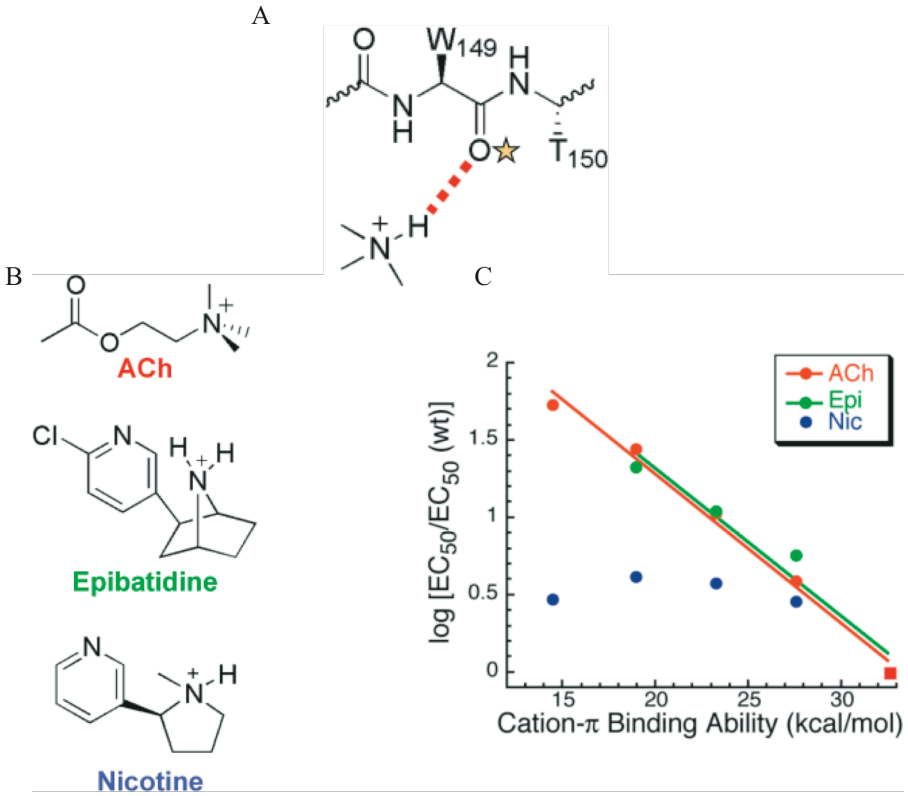

Figure 4.7. A) Schematic of the hydrogen bond between the tertiary ammonium ion of nicotine and the backbone carbonyl of αTrp149. B) Structures of three different nAChR ligands. C) Fluorination plots for ACh, epibatidine, and Nic, demonstrating the presence and absence of a cation-π interaction.

Given the previous experiments, additional agonists were investigated to further explore the difference between cholinergic and nicotinic ligand binding to the nAChR. As stated before, nicotine is a low affinity agonist at the muscle-type nAChR although it is much more potent for several of the neuronal receptors (*30, 31*). Therefore, the highly potent agonist at both muscle and neuronal nAChRs (*30, 32*), epibatidine (Epi), was also studied using the F_n-Trp series and demonstrated the presence of a cation-π interaction at

αTrp149 (*33*). As such, epibatidine serves as a probe of "nicotinic" interactions for the nAChR. It is similar in structure to nicotine although it contains the potency of ACh, making it an appropriate probe for studying nicotinic interactions at the binding site (Figure 4.7).

4.1.4 Computational Modeling of nAChRs

Many advances since the early 1970's allow for detailed experimentation exploring structure/function relationships in ion channels. The use of unnatural amino acids provides one of these tools, which helps us gain a more thorough understanding of these proteins. Another method of analysis involves using computational (*in silico*) models of either the entire LGIC or portions of the LGIC. Several types of modeling are often employed, varying in both computational intensity and accuracy. Some of those used in our lab are *ab initio* quantum mechanics (QM) and molecular mechanics force fields resulting in molecular dynamics (MD) simulations. QM calculations are very precise, computationally intensive calculations that allow for the calculation of interactions between individual molecules. On the other hand, MD simulations are much less precise, but allow for calculations on larger proteins and solvent molecules (*34, 35*). One major drawback to MD simulations is the reliance on MM force fields, which do not accurately represent many non-covalent interactions because they do not explicitly treat electrons (*36, 37*). Nevertheless, we generated models of the extracellular domains for both the neuronal α7 nAChR and the mouse muscle nAChR utilizing the most recent AChBP crystal structure and produced MD runs using these models. These models provided "dynamic" information about different chemical-scale interactions involved in maintaining the structure of the agonist binding site. In particular, we explored the role of a conserved aspartate, αD89, in shaping the aromatic box.

4.1.5 Project Goals

A critical feature of nicotine as an agonist is the extreme difference in potency between the muscle and neuronal nAChRs (*32, 38*). Nicotine is a very potent agonist for the neuronal nAChRs and has been implicated in a number of neurological diseases. In addition to its obvious role in nicotine addiction, it also plays a role in Alzheimer's and

Parkinson's disease, making it an interesting drug target (*39*). Nicotine and ACh have similar EC_{50} values (concentration of drug required to activate 50% of the channel current) for the neuronal receptors, particularly α4β2 (*40, 41*). However, nicotine is not a potent agonist for the muscle nAChR. The EC_{50} for nicotine at the muscle receptor is approximately 70-fold greater than that of ACh (Table 4.1) (*32*).

Table 4.1 EC_{50} Values for wild type muscle and neuronal nAChRs. The mouse muscle data was aquired in the Dougherty lab (*33*) and the Human α4β2 data was obtained from references (*41*)[a] and (*42*)[b].

Ligand	Mouse Muscle	Mouse Muscle β9'	Human α4β2
ACh	50 μM	0.33 μM	3.3 μM[a]
Nic	>500 μM	30 μM	3.9 μM[a]
Epi	13 μM	0.6 μM	43 nM[b]

Unfortunately, the low affinity of the muscle nAChR for nicotine is a complication that makes experimentation on this receptor with nicotine difficult due to the high concentrations of nicotine required in order to obtain electrophysiological data. The binding difference between the agonists complicates the challenge of understanding the binding modes of these small molecules to the receptor, which is important when designing drugs to modulate receptor function. The goal of these studies was to determine the residues underlying subunit specificity for nicotine binding to allow for better drug design that could target each receptor subtype. At the time of the study expression of neuronal receptors in the heterologous Xenopus oocyte was not feasible. However, recent advances have allowed incorporation of unnatural amino acids into several neuronal nAChRs (*43*).

4.2 Results

4.2.1 Conventional Mutations of the Outer Shell of the mouse muscle nAChR Binding Box

The first approach taken to determine the subunit specificity of nicotine binding involved scanning the sequence alignment between the neuronal and muscle nAChR subunits (Figure 4.8). The focus of our experiments was directed on the α subunit, which contributes to the primary face of the binding site. We used sequence alignments to determine residues that were significantly different between the receptor types, for example if there was a charged amino acid in place of a hydrophobic residue, etc. Since the aromatic binding box is conserved throughout all types of nAChRs, this would suggest that there are structural subtleties introduced by amino acids other than those directly contributing to the binding pocket. As such, it is likely that the residues that form the binding site involve a more complex organization of interactions that help to shape the "aromatic box" in such a way that facilitates or destabilizes certain binding interactions. Further, these residues may be key to understanding the difference in agonist potency and specificity between the muscle and neuronal receptors, or even between the different neuronal subunits.

Figure 4.8 Alignment of nAChR subunits including several α subunits (muscle and neuronal) and β2, δ, and γ. We introduced mutations at the residues denoted by a red asterix.

When studying low potency agonists or nAChRs where mutations reduce receptor activation, we introduce a "background" mutation that compensates for this decrease in ligand potency. A Leu-to-Ser mutation in the M2 transmembrane region of the β subunit

at a position known as 9' produces a hypersensitive receptor (*44-46*). The β9' (a distinction between β9' and "regular" wt is made) mutation is almost 50Å from the agonist binding site, located in the channel pore and has been shown to lower agonist EC_{50} values by 40-fold without altering any other trends (*45*). As such, it is important to remember that EC_{50} is a measure of channel function and is representative of equilibria between binding and gating, not just a measure of agonist affinity. Often the trends that we observe in EC_{50} are a result of changes that are due to the agonist binding interaction and not due to gating processes.

Previous studies indicate that the amino acids surrounding the aromatic box are clearly involved in determining the potency of different agonists and likely influence the binding of the same agonist at different receptor subtypes (*30*). Amino acids directly adjacent to the conserved aromatic box were evaluated for conservation of charge, size, and chemical properties. Residues αS191, αT196, and δD59/γE57 are all physically near the aromatic box based on the AChBP structure. Additionally, these residues are not conserved between nAChR subunits, such as α4β2, as seen in the subunit alignment (Figure 8). Conventional mutagenesis was used to mutate these residues to the corresponding amino acids of the α4β2 subunits. Since α4β2 receptors bind nicotine with a greater potency than muscle, we hypothesized that the mutations would allow the muscle receptor to have an equal potency for nicotine and ACh (i.e. increase the potency of nicotine relative to ACh). The mutant receptors were characterized by electrophysiology (Figure 4.9).

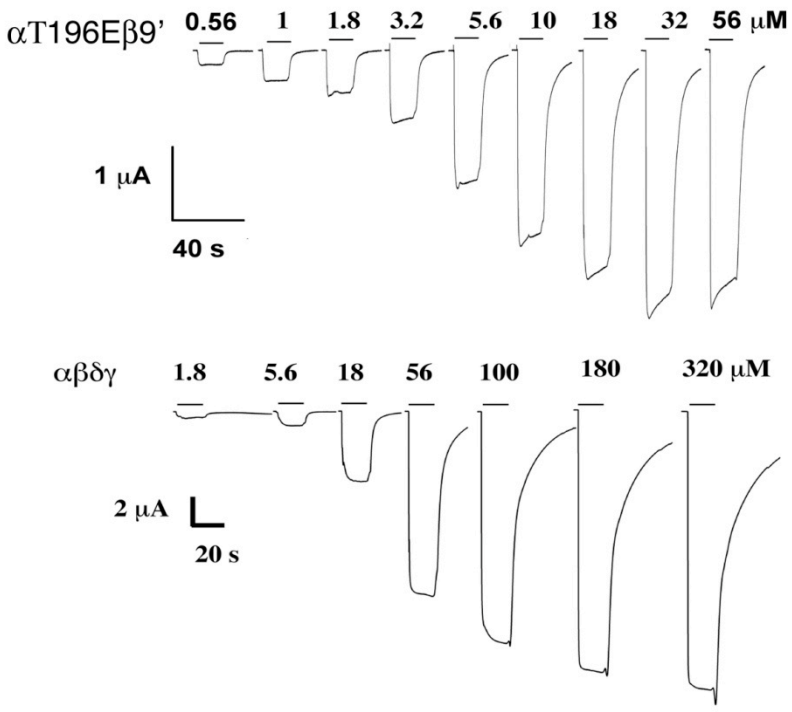

Figure 4.9 Electrophysiology traces of the inward current produced from mutant receptors αT196Eβ1δγ receptors and wild type muscle nAChRs in response to increasing doses of ACh.

Mouse muscle nAChR αS191 and αT196 are polar and hydrophilic groups containing hydroxyl side chains that have the potential to hydrogen bond. However, in the neuronal nAChRs, α191/196 are acidic residues, mostly glutamate (Figure 4.8). We hypothesized that introducing a charged side chain at these sites could create ionic interactions that shape the box allowing nicotine to be a more potent agonist. One goal of these experiments is to increase nicotine potency at the muscle nAChR relative to ACh. This approach examines the significant differences among the side chains near the aromatic box to determine their potential contributions towards agonist binding. Additionally, residues in the δ/γ subunits near the complementary face of the binding box were also significantly different when comparing the muscle and neuronal receptors. The residues δD59 and γE57, which are both acidic, were mutated to glutamine, a polar and hydrophilic amino acid that does not contain a negative charge. In the crystal structure of AChBP the amino acids in the α subunit are facing the extracellular matrix, however these residues are likely not aligned identically in the muscle type nAChR. In fact, these

residues may be able to participate in non-covalent interactions with other residues that surround the aromatic box, shaping the binding pocket.

We introduced several side chain mutations at these sites, the single mutations αS191E and αT196E, the double mutation αS191E T196E**,** and we combined the α-subunit mutations with those in δ/γ, δD59Q and γE57Q. By combining the α-subunit mutations with the δ/γ mutations we were able to study the combined effects of mutations to both faces of the agonist binding site for ACh and nicotine. These recordings were made in the presence and absence of the β9' mutation as well, to ensure that we were recording accurate responses from the mutant receptors with both traditional wild type and the β9' wild type (Table 4.2). Plots of the ratio of EC_{50} for the mutant receptors compared to the EC_{50} for the wild type receptor demonstrate the change in receptor potency for both ACh and nicotine (Figure 4.10). As a reference the EC_{50} values for α4β2 wild type receptors were also plotted against the muscle receptor. This provides a "baseline" for which we can compare our mutated muscle receptors since one goal is to make a muscle receptor respond to nicotine similarly to the neuronal nAChRs.

Table 4.2 EC_{50} data for mutations of the outer shell residues near the muscle nAChR binding site.

Mutations	EC_{50} μM ACh	Hill Value (ACh)	EC_{50} μM Nic	Hill Value (Nic)
WT	57	1.17	>500	N/A
αT196E	2.5	1.65	75	1.48
αS191E	2	1.01	82.2	0.88
αS191E T196E	10.5	1.45	350	0.93
αT196EδγE57Q	3.6	1.95	101	1.76
αT196EδD59Qγ	7.5	1.34	135	1.41
αT196EδD59QγE57Q	11.3	2.04	111.5	2.21
WTβ9'	0.33	1.34	30	1.52
δD59Qβ9'	-	-	77	1.26
γE57Qβ9'	-	-	75	1.76
αT196Eβ9'	0.35	1.7	3.8	1.43
αS191Eβ9'	0.42	0.89	6.5	2.07

All of the mutations introduced into the α-subunit and the δ/γ subunits resulted in a decrease in EC_{50} value for both ACh and nicotine (Figure 4.10). However, using α4β2 wild type values for comparison, none of the mutations resulted in producing a muscle

receptor with the same potency for ACh or nicotine as a neuronal receptor. The goal of these studies was to obtain a mutant receptor that had the same EC_{50} for ACh and Nic, making them more neuronal-like in function. The largest shift was obtained for the αT196E mutation, which resulted in a 8-fold shift for nicotine and 12-fold shift for ACh. Interestingly, this site appears to affect ACh more than Nic, and turns ACh into a more potent agonist than it is at the wild type α4β2 receptor (Figure 4.10).

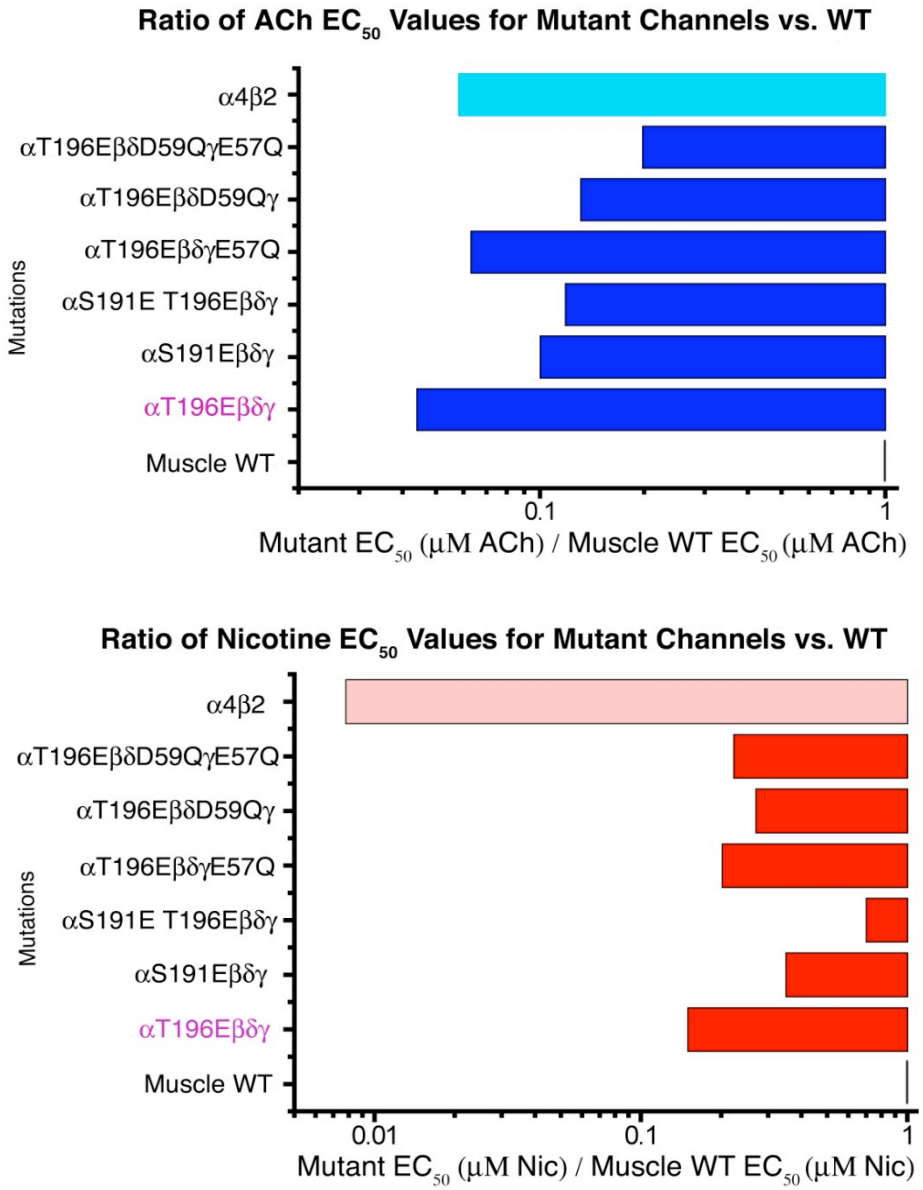

Figure 4.10 Ratio of EC_{50} values for binding site mutants vs. wild type muscle nAChR in response to ACh (blue) and nicotine (red). The EC_{50} for wild type α4β2 is shown (light blue and red, respectively) as a reference.

Combining the α-subunit mutations with δ/γ mutations generally resulted in larger decreases in EC_{50} (increase nicotine and ACh potency) than with the single mutations. This was particularly evident by the αT196E mutant, which shifted more when combined with other mutations (Table 4.2, Figure 4.10). Residues homologous with α196 lie directly behind α198 in the AChBP crystal structure, and α198 is one of the aromatic box residues that make direct contact with the agonist (*22*). In AChBP the αT196 homologue is exposed to solvent, which suggests that a charged side chain such as glutamate would be even more stable than threonine in the solvent-exposed hydrogen-bonding environment. The crystal structure does not indicate a clear bonding partner for α196, however it remains a possibility that the muscle receptor residues in this area are not solvent exposed, but instead making intrasubunit contacts. We assume that the structure of muscle nAChR is similar to AChBP, but it is not likely that all the side chains are oriented in the same direction in both proteins. This does not explain the decrease in EC_{50} values we observe for both ACh and Nic, and there is no obvious reason why mutating αT196 alters ligand potency.

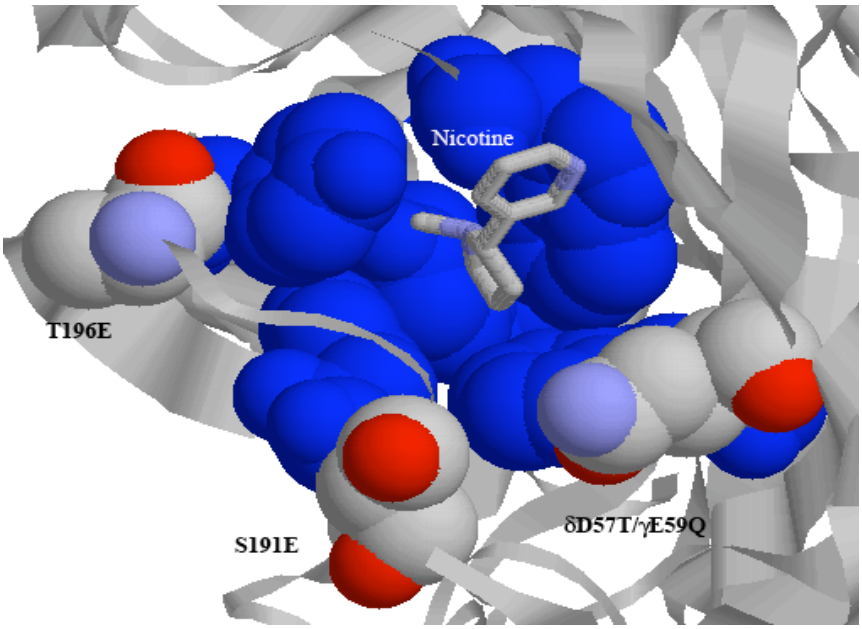

Figure 4.11. Binding site of AChBP with nicotine bound to the aromatic box. Mutations are shown in CPK colors and the aromatic box residues are blue.

There are additional reports that other non-α subunit residues, δD59N and γG57S (similar to the above reported mutations), when mutated, demonstrate decreased affinity for ACh (*32*). Interestingly, these non-α amino acids form the lower part of the binding site, according to the AChBP structure (Figure 4.11). Carbamylcholine (another choline agonist) binding is influenced by δD59 and γE57, but that amino acid does not appear to influence ACh or nicotine binding (*47*). However, our mutations in δ/γ did not result in a large increase (or decrease) in ACh or nicotine potency.

4.2.2. Chimera Experiments Between Mouse Muscle and Neuronal nAChRs

Although the α196 mutant increased muscle nAChR potency for nicotine, it did not increase the potency to equal that of the neuronal receptors. We thought that expanding our region of analysis to include additional residues in the outer binding shell could result in larger EC_{50} shifts. To investigate whether the effects of larger scale alterations to the outer shell of the binding pocket would induce a larger shift in potency we examined several "loop" areas in the extracellular domain previously implicated in determining agonist specificity and generated chimeras (mutant receptors containing segments from at least two different subunits) between the muscle and neuronal receptors.

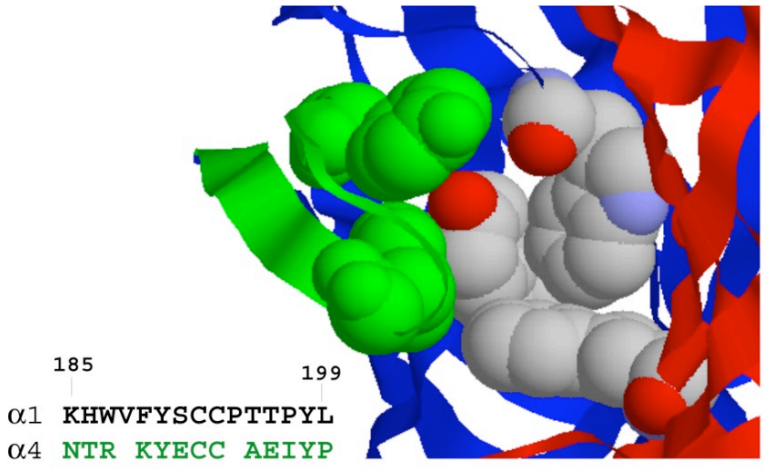

Figure 4.12 Alignment of β9-β10 loop from muscle α1 and neuronal α4 subunits. The loop is highlighted in green in the AChBP structure and is directly adjacent to the aromatic box, and includes αY190 and αY198, two aromatic box residues.

Previous experiments constructed chimeras between the α4 and α7 neuronal nAChR subunits (*4*). These chimeras focused on residues α186-α194, which are in a loop identified to contribute in part to some of the differences in agonist specificity between the neuronal α7 and α4β2 receptors (*4*). This loop, the β9-β10 loop, contains the α196 residue described above which we found to alter nicotine potency, therefore it is reasonable to infer that this region shapes the agonist "box" and could make the mouse muscle receptor more sensitive to nicotine.

To increase agonist potency at the muscle type nAChR, we constructed a chimera between mouse muscle $(\alpha 1)_2\beta 1\delta\gamma$ and the human α4β2 receptor at the β9-β10 loop area (Figure 4.12). The α subunit chimera was expressed in oocytes with wild type β, δ, and γ subunits. Unfortunately, protein expression was very low for these receptors and responses to ACh and nicotine could not be reliably obtained. One possibility is that this loop is important for receptor assembly, therefore substantial mutations prevent proper ion channel formation. Additionally, it is possible that this region of the protein is important for receptor trafficking, and our mutations prevented the ion channels from reaching the cell surface. Since the chimera did not express we decided to make several point mutations within the chimera loop. We wanted to explore the role of several nonconserved amino acids in shaping the aromatic box. The mutations αV188L, αV188K, and αL199P were constructed, however all of these mutations produced ion channels with little to no expression in response to ACh or nicotine.

4.2.3 Unnatural Amino Acid Mutagenesis of Outer Shell Amino Acids

Our previous efforts to understand how contributions from the outer binding shell amino acids contribute to agonist specificity remained unclear; therefore we turned to exploring the role of hydrogen bonds in shaping the aromatic box. Using unnatural amino acid mutagenesis we can introduce subtle mutations to alter hydrogen-bonding properties of the amino acid side chains. A nAChR conserved Trp, αW86, was previously studied for its role in a potential cation-π interaction with ACh (none was found), but the hydrogen bonding potential of the indole N-**H** was not investigated. αW86 is in close proximity to another conserved residue, αD89, in the AChBP crystal structure, which has been

implicated in shaping the binding site (*29*). We were interested in exploring the potential hydrogen bond between αW86 and αD89 in mouse muscle nAChR (Figure 4.13).

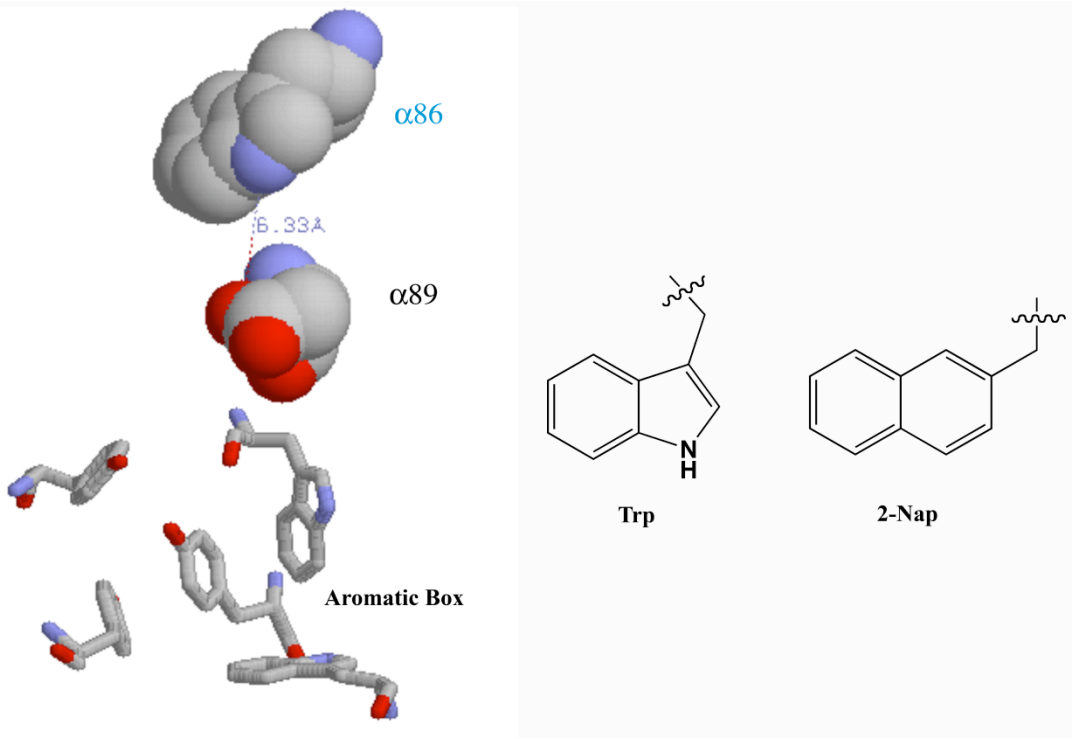

Figure 4.13 Potential hydrogen bond between αW86 and αD89 involved in shaping aromatic box. Hydrogen bonds in Trp can be probed by introducing the unnatural amino acid 2-napthylalanine (2-Nap).

A Trp derivative, 2-napthylalanine (2-Nap, Figure 4.13) was incorporated into the αW86 residue of mouse muscle nAChR to investigate the importance of this position as a hydrogen bond donor with its potential proximal partner, αD89. The derivative, 2-Nap is similar in size and structure to Trp, but does not contain the hydrogen bond donor (N-H) in the indole ring. However, 2-Nap retains the aromaticity of the natural Trp sidechain, and allows us to probe the hydrogen bond characteristics of αW86 without significantly altering the electronic aspects of the side chain.

Incorporation of αW86 2-Nap did not result in an EC_{50} shift for ACh. If the hydrogen bond were important for shaping the aromatic box we would expect a rightward shift in EC_{50}, which was not observed (Figure 4.14). One difference upon 2-Nap incorporation is an increase in the Hill coefficient, which is an indication of the

cooperativity between the binding sites of the receptor. This higher Hill coefficient suggests that there is more cooperativity between the binding sites when 2-Nap is incorporated compared to Trp. This suggests that this residue may be important for gating interactions or conferring conformational changes between subunits of the receptor. Hydrogen bonding and the cation-π interaction are not requirements of αW86, yet this Trp is conserved in all α subunits, suggesting that this residue plays a role in maintaining correct protein structure. To test this hypothesis we incorporated an alanine residue at α86, which completely obliterates the side chain. The αW86A mutation drastically decreased the amount of currents generated in response to ACh, suggesting that this is a structural residue, however EC_{50} values could not be determined. This result is consistent with the hypothesis that a large, hydrophobic amino acid is structurally important at this highly conserved site.

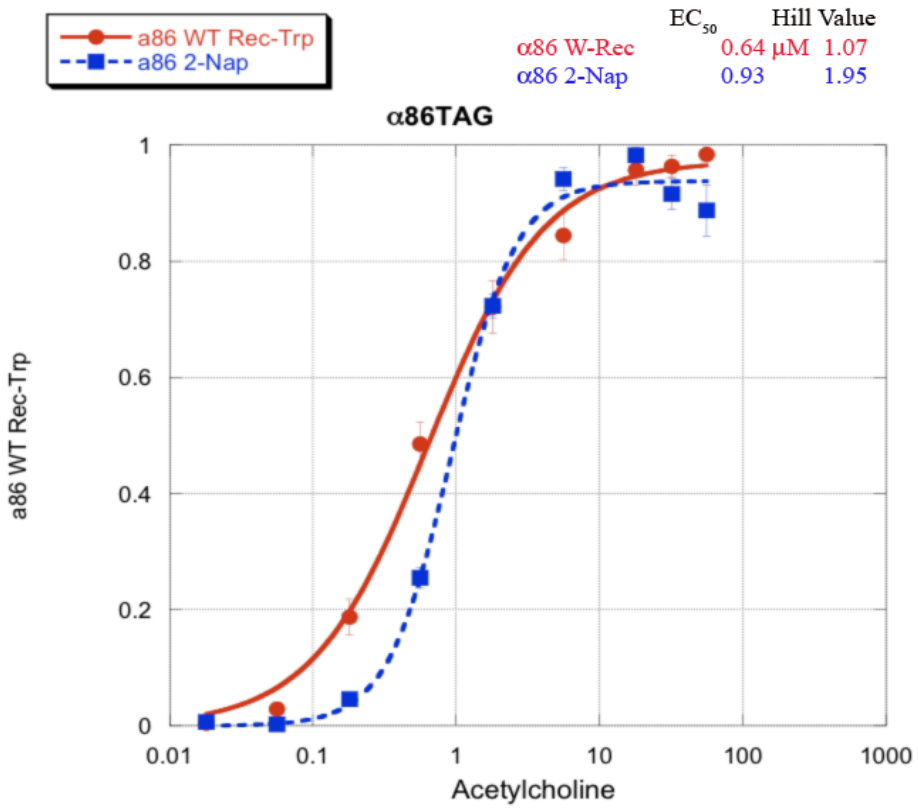

Figure 4.14 EC_{50} plot of α86 wild type recovery and α86 2-Nap data demonstrating no shift in EC_{50}.

Two additional, highly conserved residues that physically surround the aromatic box were also examined in the α subunit. The residues, αP21 and αY151 were mutated in order to determine the importance of their conservation in receptor function. These residues are positioned on either side of α86 in the AChBP structure, suggesting that these conserved residues could interact with one another during agonist binding and/or the receptor gating process.

We perturbed αY151 by incorporating the unnatural amino acid 4-Me-Phe which is sterically similar to Tyr but unable to form hydrogen bonds since it lacks both a hydrogen bond donor and acceptor. Tyr is conserved at this position throughout all nAChRs as well as several other Cys-loop family receptors. Since Tyr is both a hydrogen bond acceptor and donor we wanted to test the implications of altering these characteristics at this site by replacing the hydroxyl with a methyl group. We hypothesized that αT151 4-Me-Phe would be worse at structuring the aromatic box, resulting in EC_{50} shifts to the right (decreasing agonist potency). Replacement of the hydroxyl with a methyl group did shift EC_{50} rightward approximately 5-fold for both ACh and nicotine (Table 4.3). This suggests that the hydroxyl plays an important role in hydrogen bonding at that site, possibly influencing the general shape of the aromatic box for both cholinergic and nicotinic agonists.

Table 4.3 EC_{50} data for mutations of conserved residues, α151 and α21 in mouse muscle nAChR.

Mutations	EC_{50} μM ACh	Hill Value (ACh)	EC_{50} μM Nic	Hill Value (Nic)
WTβ9'	0.33	1.34	30	1.52
αY151TAGβ9' Phe	3.8	2.08	-	-
αY151TAGβ9' 4-Me-Phe	2.04	1.71	154.6	1.86
αP21Fβ9'	1.05	2.45	100.5	1.68
αP21Gβ9'	0.7	1.51	13.9	1.47

The conserved proline, α21, is present in all Cys-loop family receptors. The orientation of αP21 above αW86 (in AChBP) suggests that αP21 is another structural residue that holds the formation of the residues in the outer shell of the binding box in

place. In general, prolines are rigid and often found in protein turns because they can induce a kink within helices. Since proline residues provide a distinct structure-function relationship, we were interested in determining if this proline residue played a role in structuring the agonist binding site. We introduced the conventional mutations, Phe and Gly, at α21. Incorporation of the large, aromatic group, αP21F, resulted in a 3-fold shift in EC_{50} for both ACh and Nic. The more interesting effect came with the αP21G mutation, which resulted in a 2-fold increase in EC_{50} for ACh while lowering that of nicotine 2-fold. These results suggest that "locking" the binding site into one conformation (Phe mutation) reduces overall agonist potency while introducing a more flexible residue (Gly mutation) is more beneficial for nicotine binding, possibly allowing the binding site to accommodate the different steric constraints of nicotine. The mutation αP21G results in an increase in nicotine potency, which suggests that nicotine might require a larger box structure in order to bind more tightly to the receptor. Proline could constrain the binding site and the increased flexibility introduced by glycine may allow the binding site to reorient around nicotine for a better "fit." The conservation of αP21 in all nAChR subtypes suggests that although this amino acid is important for structuring the aromatic box, it does not likely define subtype specificity between muscle and neuronal nAChRs.

4.2.4 A Computational Model of Extracellular Domain of Mouse Muscle nAChR

The goal of these experiments was to generate models of the entire binding site (all outer shell residues) of the nAChR. The structure of AChBP provides a good model for the extracellular domain, yet there is good reason to believe that it does not accurately describe the structure of the binding site in the nAChRs, especially the heteromeric receptors. Previous models have been generated using different templates, alignments, and structural refinements; producing similar yet subtly different results (*27, 28, 48-50*). The variations in the binding between ACh, nicotine, and epibatidine for the different receptor subtypes also indicate that many differences must be present in each receptor. Ideally, we could generate models of the binding site that take into account these differences and not just evaluate the conserved aromatic residues. We need to account

for the outlying residues, the equivalent to the first and second solvation shell of a small molecule, which impart the differences contributing to ligand specificity.

A model for the human α7 homomeric nAChR extracellular domain was generated by E.J. Petersson (*51*). This model used the backbone architecture of the AChBP structure as a basis for "threading" on the α7 subunit sequence. The α7 homology model was generated using the AChBP structure with nicotine bound (Subunit A, of 1UW6). Refinements were made to the structure and then MD simulations were performed to generate several nanoseconds of movement of the extracellular domain of the α7 LBD. We utilized this model of α7 as a guide to generate a model of the mouse muscle extracellular domain $\alpha 1_2\beta\delta\gamma$.

Figure 4.15 A) Alignment of the alpha subunit from *Torpedo marmorata* with α1 mouse. The beginning and end of the LBD sequence in the final PDB file is denoted by (*).

We constructed sequence alignments between *T. marmorata* from Unwin's model of the nicotinic receptor (*12*) and the different mouse muscle subunits using the program T-coffee (*52*); Figure 4.15 has examples of the α subunit alignments. *T. marmorata* has almost exact sequence homology to the mouse muscle receptor subunits therefore, the fit was ideal. The program Prime, part of the Schrodinger (*53*) suite of software, was used to develop a homology model based on the *T. marmorata* structural model, PDB file 2BG9 (*10, 12*). We generated three models of α7 and mouse muscle (mm_nachr), one without ligand, one with nicotine bound, and one with carbamylcholine (CCh) bound.

A single subunit of *T. marmorata* (without ligand) was used as a template for generating mm_nachr. During the build step side chains were allowed to move. Each subunit was built and exported individually and exported as a PDB file. A pentamer was built in Swiss PdbViewer (*54*) by aligning each subunit onto the *T. marmorata* pentamer. The pentamer was exported back into Prime, where loop refinement algorithms and side chain predictions were performed. We performed refinements for the C loop, which is directly implicated in forming the binding site in nAChRs. Residues homologous among the mm_nachr subunits and *T. marmorata* were held fixed. The final chain assignments were made, Chain A (α1), Chain B (δ), Chain C (β), Chain D (α), and Chain E (γ). Chain A of the Torpedo structure was used as the template for both of the α subunits of the mouse muscle nAChR This pentamer was then exported as a PDB file to GROMACS for molecular mechanics minimizations (*54*).

The mm_nachr heteropentamer was converted to a GROMACS format for molecular mechanics. The pentamer was placed in a hexagonal periodic box with 7 Å gaps between the edge of the box and the protein. Explicit solvation was added to the box using SPC water molecules (*55*), followed by the addition of ions (Na^+ and Cl^-) to the box at a concentration of 150 mM. Extra Na^+ ions were added to the box to neutralize the -62 total charge of the protein.

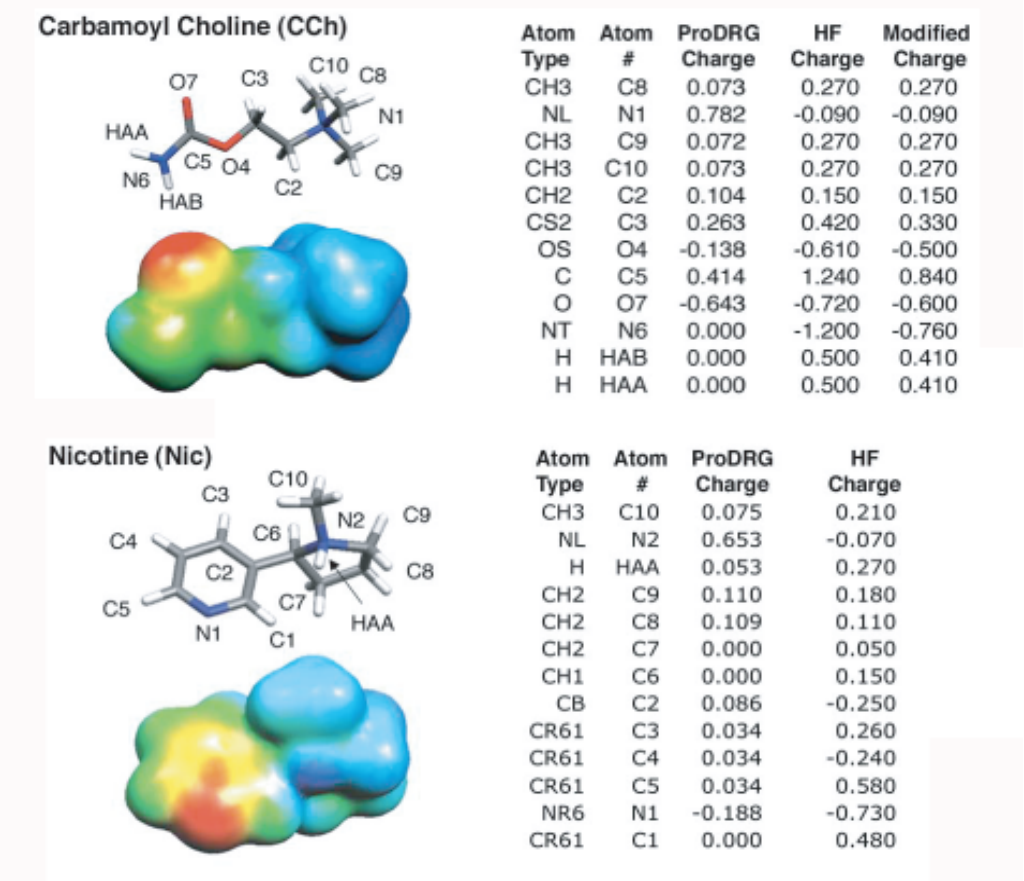

Atom Type	Atom #	ProDRG Charge	HF Charge	Modified Charge
CH3	C8	0.073	0.270	0.270
NL	N1	0.782	-0.090	-0.090
CH3	C9	0.072	0.270	0.270
CH3	C10	0.073	0.270	0.270
CH2	C2	0.104	0.150	0.150
CS2	C3	0.263	0.420	0.330
OS	O4	-0.138	-0.610	-0.500
C	C5	0.414	1.240	0.840
O	O7	-0.643	-0.720	-0.600
NT	N6	0.000	-1.200	-0.760
H	HAB	0.000	0.500	0.410
H	HAA	0.000	0.500	0.410

Atom Type	Atom #	ProDRG Charge	HF Charge
CH3	C10	0.075	0.210
NL	N2	0.653	-0.070
H	HAA	0.053	0.270
CH2	C9	0.110	0.180
CH2	C8	0.109	0.110
CH2	C7	0.000	0.050
CH1	C6	0.000	0.150
CB	C2	0.086	-0.250
CR61	C3	0.034	0.260
CR61	C4	0.034	-0.240
CR61	C5	0.034	0.580
NR6	N1	-0.188	-0.730
CR61	C1	0.000	0.480

Figure 4.16 Charges generated for the agonists, CCh and Nic. The ProDRG charges are listed and the modified charge determined using Hartree-Fock (HF) calculations, which were determined by HF/6-31G** computations. These also produced the electrostatic potential surfaces that correspond to an energy range of $^{+}$10 to $^{+}$130 kcal/mol (blue is more positive and red is less positive).

We generated three separate mm_nachr models, one without ligand, and two with ligands (Nic and CCh). Into the mm_nachr model we inserted either nicotine or CCh at the two binding sites, α/δ and α/γ. This was performed by aligning the binding site of the AChBP structure with nicotine (1UW6) and CCh (1UV6) with the mm_nachr pdb file. We generated the parameters for nicotine and CCh using the ProDRG (http://davapc1.bioch.dundee.ac.uk/programs/prodrg/) website, although the charges it generated were determined to be unacceptable because it placed most of the positive charge on the nitrogen atoms of the ammonium groups (*56*), therefore modified charges were used (Figure 4.16). The modified CHELPG charges from HF/6-31G** calculations

were used for nicotine (*57*). In the case of CCh, the partial charges generate large intramolecular forces between carbamyl oxygens and protons, which GROMACS cannot resolve. Therefore these charges were lessened and labeled as the "Modified Charge" in Figure 4.16. The Nic-bound and CCh-bound mm_nachr proteins were also placed in periodic boxes containing solvation and counterions, as described above.

The three mm_nachr proteins (apo, Nic, and CCh bound) began with seven minimizations prior to the MD simulations:

Minimization 1: Identical residues frozen, protein (ligand) strongly restrained
Minimization 2: Identical residues frozen, protein backbone strongly restrained
Minimization 3: Identical residues frozen, protein backbone weakly restrained
Minimizaiton 4: No residues frozen, identical residues strongly restrained
Minimization 5: No residues frozen, identical residues weakly restrained
Minimization 6: All non-hydrogen atoms strongly restrained
Minimization 7: Completely unrestrained proteins

The resulting minimized structures were the basis for our MD simulations using the GROMACS force field. We began the MD simulations at 0 K, and slowly warmed up to 310 K, using a linear annealing function over the first 25 ps of simulation time. The protein (and ligand, when present) was held under strong restraints during the warm-up sequence and over the next 125 ps the restraints were relaxed. The system began to equilibrate (energies leveled out) after the first 1 ns of run time.

4.2.5 Computational Studies of the Mouse Muscle nAChR Binding Site

The mouse muscle homology model was used to evaluate several intrasubunit chemical interactions that form the agonist binding site. Previous mutagenesis studies demonstrated that interactions between muscle receptor D89 and loop B residues (Figure 4.17) influence the binding of ACh and epibatidine differently than Nic (*58, 59*). Incorporation of several unnatural amino acids at D89, Nha and Akp, and at loop B residues W149 and T150 (alpha hydroxy acids tryptophan alpha hydroxy acid (Wah) and

threonine alpha hydroxy acid (Tah), respectively) resulted in different EC_{50} shifts for ACh, Epi, and Nic (*59, 60*).

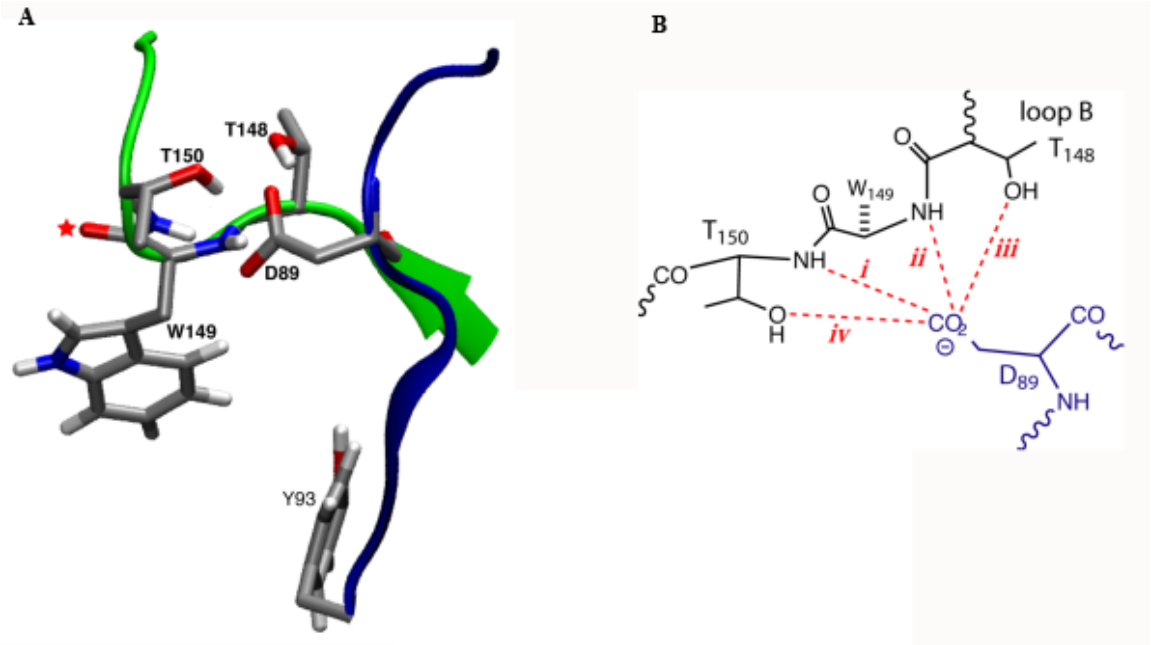

Figure 4.17 A) Image of the agonist binding site including the positioning of D89 and Loop B residues, T150 and T148. B) Schematic of potential hydrogen bonds (*i-iv*, red) between D89 (loop A, blue) and Loop B residues.

This hydrogen bonding network (Figure 4.17B) was perturbed most significantly by the D89N mutation, which eliminated the negative charge, eliminated a hydrogen bond, and introduced a possible dipole-dipole clash $N^{\delta-}–H^{\delta+}\bullet\bullet\bullet H^{\delta+}–N^{\delta-}$. This mutation increased EC_{50} for both ACh and epibatidine, suggesting that hydrogen bonds *i* and *ii* were most influential during binding (Figure 4.17B). Additionally, double mutations between D89N/T150Tah and D89N/W149Wah were performed. The D89N/W149Wah mutation recovered wild type receptor activity, but D89N/T150Tah did not. These indicate that the hydrogen bonding network is asymmetric in its contributions to the agonist binding site (*59, 60*).

To further investigate this hydrogen bonding network the homology model of the mouse muscle extracellular domain was utilized to study these interactions. The mm_nachr models with CCh and without were used to monitor hydrogen bonds *i* through

iv analyzing both carboxylate oxygens (named OD1 and OD2) shown in Figure 18, resulting in a total of 8 possible hydrogen bonds. Two additional "control" hydrogen bonds within a well defined α helix were also monitored.

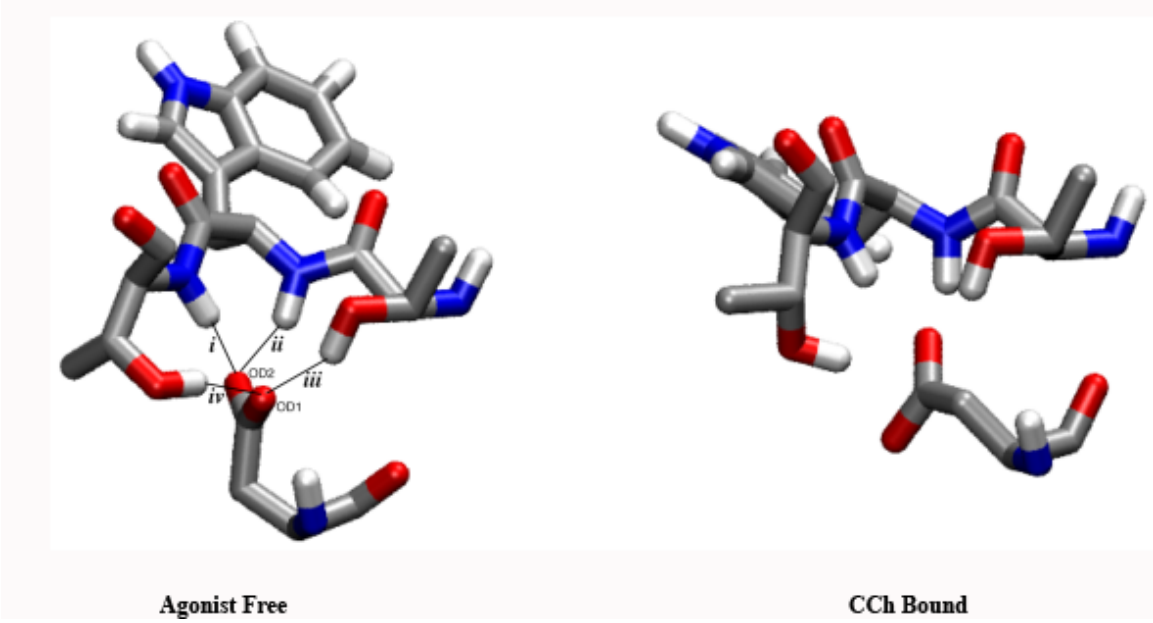

Figure 4.18. Agonist free and CCh bound structures of the mouse muscle agonist binding site from the homology model (mm_nachr). The structures were generated using the GROMACS g_cluster program taken from the final 500 ps of the 5ns mm_nachr MD simulations.

In the agonist free structure one of the carboxylate oxygens, OD2, makes hydrogen bonds with the backbone NH groups, *i* and *ii*. The other carboxylate, OD1, makes hydrogen bonds with the side chain hydroxyls, *iii* and *iv* (Figure 4.18). These are strong hydrogen bonds that frequently appear in the MD simulations, meaning they do not fluctuate (relative to the control hydrogen bonds). In contrast, when CCh is bound these hydrogen bonds begin to fluctuate significantly, being present only 34% of the time versus 94% in the agonist free structure. Overall, this difference is mostly observed between hydrogen bonds *i* and *ii* while *iii* and *iv* remain present (Figure 4.19). Additionally, the distance between D89 and W149 increases when agonist is bound. The MD simulations indicate that D89 is rotated into a less symmetrical position with respect to loop B upon agonist incorporation.

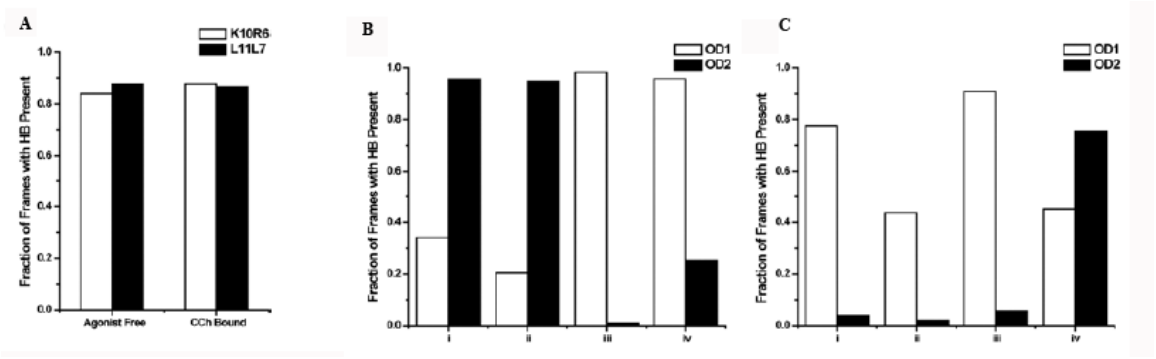

Figure 4.19 A) The "control" hydrogen bonds monitored between backbone amine of K10 and the backbone carbonyl of R6 (white bar) and backbone amide of L11 and backbone carbonyl of L7 (black bar). The hydrogen bonds (8) analyzed for the agonist free (B) structure and the CCh bound structure (C) are shown between OD1 (white) and OD2 (black) carboxylate oxygens. All of the data were acquired during the equilibrated final 500 ps of the 5 ns MD simulations. Data are expressed as the numbers of frames out of 1000 observed frames where the given hydrogen bond is present.

The mutagenesis studies performed by Sine and coworkers (*58*) established that the D89N mutation affects the kinetics of the association between the agonist and the unbound receptor. Therefore, we used our homology model to generate a new mm_nachr structure containing the D89N mutation, which we used for analysis of the hydrogen bonding network. We only constructed a model in the agonist free state since the mutation is implicated in the kinetics prior to agonist binding. Due to the orientation of the D89N mutation, we considered two different models labeled D89N1 and D89N2, which correspond to the positioning of the amide nitrogen relative to OD1 or OD2, respectively. Introduction of the D89N mutation disrupted the interactions between loop B and the side chain. In the agonist bound structure there are an average of 4.7 hydrogen bonds between the side chain and loop B, while in the D89N mutant there are ~1.5 hydrogen bonds (many are different than the original *i-iv)* (Table 4.4). These results indicate the importance of this hydrogen bonding network during agonist binding and establish important chemical-scale interactions between D89 and loop B.

Table 4.4 Molecular dynamics simulations of the D89/Loop B hydrogen bonds.

Structure	D89/Loop B Distance (Å)[a]	Mean # of D89/Loop B Hydrogen Bonds[b]	Loop B RMSD (wt vs. mutant)[c]
wt agonist free	4.3 ± 0.2	4.7 ± 0.8	-
wt CCh bound	5.2 ± 0.3	3.4 ± 0.8	-
D89N1	5.3 ± 0.3	1.6 ± 0.6	2.5 ± 0.1
D89N2	8.1 ± 0.5	1.5 ± 0.9	3.8 ± 0.3

All data were acquired over the last 500 ps of each simulation and are reported as the mean ± standard deviation. [a]Distance measured between D/N89 (γ carbon) to the W149 α carbon. [b]All hydrogen bonds *i-iv* including both OD1 and OD2. [c]RMSD is calculated compared to the averaged last 500 ps from the agonist free wild type mm_nachr simulation. The average structure was determined using the program g_cluster.

4.3 Discussion and Conclusions

The muscle and neuronal nAChRs have many similarities, particularly with respect to the conservation of the aromatic box amino acids. However, there are many more subtle structural differences that contribute to agonist specificity, particularly nicotine, between these receptors that are a challenge to uncover. Conventional mutagenesis studies were performed to make nicotine a more potent agonist for the muscle nAChR. The introduction of a charged residue at αT196 provided the greatest increase in potency of the muscle nAChR for nicotine. Although this mutation does not equalize the muscle and neuronal nAChR potency for nicotine and ACh, this mutation provides enough of a shift so that analysis on the muscle receptor can be performed without using doses of nicotine that block the receptor. However, all of the mutations that increased the potency of nicotine increased that of ACh as well.

In the unnatural amino acid studies, it is surprising that altering the hydrogen bonding properties of several of the conserved residues in the extracellular domain of the nAChR did not alter agonist potency. This suggests that many of the conserved amino acids outside of the "box" are not as structurally important as the conserved residues that compose the agonist binding site. A more accurate description is that these outer box residues are important for shaping the agonist binding site, however individually they contribute less than the aromatic box residues to agonist binding.

After these initial studies, further mutagenesis was performed on several of these residues. One study evaluating the importance of backbone hydrogen bonds near the aromatic box discovered that the backbone N-H of S191 (one of the outer box mutations discussed above) makes an inter subunit hydrogen bond with the complementary face residues γD174/δD180 after agonist binding (*61*). This residue is important for transferring crosstalk between the subunits that contribute to the agonist binding site.

Additionally, as discussed above, a series of mutagenesis studies was performed analyzing the hydrogen bonding network surrounding the aromatic box. These studies were performed on the loop A residue, D89, which is part of the highly conserved WxPD motif in loop A of the α subunit. These studies demonstrated that no single hydrogen bond was crucial for maintaining the structure of the agonist box, yet they all contribute to forming contacts between loops A and B. Additionally, it was determined that the charge on D89 did not interact with the cationic agonist, but instead contributed to a hydrogen bonding network with the backbone amides of αW149 and αT150. Differences were also observed between the more potent agonists ACh and epibatidine as compared with the less potent agonist nicotine. Nicotine only makes one contact with loop B (*33*), and perturbations between the D89 and loop B network do not shift EC_{50} values of nicotine as much as they do for both ACh and epibatidine. Therefore, ACh and epibatidine are more sensitive to these perturbations and the outlying structure of the protein surrounding the binding site than nicotine.

The molecular dynamics simulations correlate well with the experimental data from our lab and others. Interestingly, the MD simulations suggest that D89 is positioned to interact with loop B in the agonist free structure and establishing more optimal interactions than in the carbamylcholine bound structure. Agonist binding (at least with CCh) does not dramatically shift the positioning of loop B, suggesting the agonist does not contribute to the structural orientation of the loop after binding. On the other hand, introduction of the D89N mutations into the simulation also reduces the number of interactions between loops A and B. When Asn is incorporated into the structure, loop B alters its conformation to accommodate the new side chain, however this changes its structural organization around the aromatic box. Our conclusion from these studies is

that the hydrogen bonding network between D89 and loop B originates to "preorganize" the aromatic box in anticipation of ligand binding (*62*).

Further advances and familiarity with unnatural amino acid mutagenesis have allowed for our exploration of structure/function studies with neuronal nicotinic receptors. These studies demonstrate that the cation-π interaction is conserved in the α4β2 receptor where it contributes to the high affinity for both ACh and nicotine (*43*). The aromatic box is conserved in all receptors, and a cation-π interaction is present for both ACh and nicotine in the neuronal α4β2 receptor, which has a high affinity for both agonists. Yet the muscle receptor does not utilize a cation-π interaction to bind the low affinity nicotine even though the same aromatic residues contribute to the binding site. These studies only reiterate the subtleties that contribute to the differences between nicotinic receptor subtypes.

In conclusion, all of the above studies indicate that the structural aspects of the acetylcholine receptor important for agonist specificity between muscle and neuronal types lie in the immediate vicinity outside of the "aromatic box". These amino acids ultimately shape the box to accommodate the proper orientation of agonists important for necessary receptor function. It is likely that these residues also contribute to maintaining a preferred "preorganized" structure, optimal for ligand binding. Overall, many questions remain about the interactions involved in nicotine binding to the muscle and neuronal nAChRs, and continued studies probing receptor structure and function on the chemical-scale will enable our understanding of these important neuroreceptors.

4.4 Materials and Methods

4.4.1 Mutagenesis and Unnatural Amino Acid Suppression

The mouse muscle nAChR subunits, α, β, δ, and γ were all transcribed into mRNA from the pAMV vector as previously described (*63*) by *in vitro* runoff transcription using the Ambion (Austen, TX) T7 mMessage mMachine kit. Wild type mouse muscle nAChR subunits were injected in a 2:1:1:1 ratio; nonsense suppression experiments used a 10:1:1:1 ratio of α:β:δ:γ. Unnatural amino acids and aminoacyl-tRNA were prepared using previously reported methods and conjugated to the dCA dinucleotide as described (*64*). Aminoacyl tRNA was photolyzed (5 minutes) for deprotection prior to co-injection

with the mRNA (*65*). In several of the experiments noted above, the Leu9'Ser mutation in the β subunit (β9') was used to lower all EC_{50} values by approximately 40-fold (*26, 66*). Stage V-VI *Xenopus laevis* oocytes were injected with 50nL of mRNA/tRNA mixtures per injection. All oocytes used to study the nAChR were recorded in a Ca^{2+}-free ND96 solution (96 mM NaCl, 5 mM HEPES, 2 mM KCl, 1 mM $MgCl_2$).

4.4.2 Electrophysiology

All of the electrophysiological recordings were performed on the Axon Instruments, OpusXpress™ . Stage V-VI *Xenopus laevis* oocytes were employed in all of the studies. Eight oocytes were simultaneously voltage clamped at -60 mV and dose-response relationships were obtained by delivery of various concentrations of ACh, nicotine, or Mg^{2+} in 1 mL aliquots. Oocytes were superfused with Ca^{2+} free ND96 solution at a flow rate of 1mL/min before application, 4mL/min during drug application, and washed at 3mL/min. Drug application was 15 s. Data were sampled at 125 Hz and filtered at 50 Hz. Acetylcholine and nicotine were purchased from Sigma/RBI/Aldrich. Epibatidine was purchased from Tocris as (±) epibatidine dihydrochloride. All the drugs were dissolved in sterile ddi water and diluted in Ca^{2+} free ND96. The data were analyzed using the Clampfit 9.0 software. The Hill equation was used to fit data where $I/I_{max} = 1/(1+(EC_{50}/[A]^{nh}))$, I is current peak at drug concentration (A), EC_{50} is the concentration of drug that activates 50% of the maximal response, and n_H is the hill coefficient.

4.4.3 Mouse Muscle Homology Model of D89N Mutant Structures

The D89N mutation was introduced into the mouse muscle homology model by mutating α89 to Asn in the PDB file of both α subunits in SwissPDB viewer. The two structures differed in the positioning of the NH_2 group of the side chain, D89N1 placed the NH_2 group in the same position as the OD1 group of the wild type mm_nachr structure, and D89N2 placed the NH_2 group in position with OD2. The D89N mm_nachr models were placed in a hexagonal periodic box, solvated, and treated using the same protocol developed for the wild type model.

All five of the mm_nachr structures (agonist free wt, CCh wt, nicotine wt, D89N agonist free, and D89 CCh) were treated similarly. The MD simulations were started at 0

K and warmed to 310 K over the first 25 ps of the run. Large restraints were used at first for both the protein and drug (if applicable) and slowly released over the next 100 ps. Then the protein was run unrestrained for an additional 5000 ps (wt) or 7500 ps (D89N structures). The D89N structures were generated with Michael M. Torrice and the analysis of the bonding network from g_cluster was performed by M.M.T (*60, 67*). The α7 homology model and molecular dynamics simulations were performed by E. James Petersson (*51*).

All of the molecular dynamics simulations were analyzed over the final 500 ps of trajectories to ensure equilibration of the system energies. Each of the trajectory files analyzed contained data for every 0.5 ps, producing 1000 frames/simulation. The programs g_dist and g_hbond within GROMACS were used to analyze distances and hydrogen bonds. The default cutoffs for determining hydrogen bonds were a distance of 3.5 Å with an acceptor-donor angle of 30º. RMSD values were calculated using g_rms and compared to the final 500 ps of data from the wild type, agonist free mm_nachr structure using g_cluster.

4.5 Cited References

1. Sine, S. M., and Engel, A. G. (2006) Recent advances in Cys-loop receptor structure and function, *Nature 440*, 448-455.
2. Changeux, J. P. (1983) Concluding remarks: on the "singularity" of nerve cells and its ontogenesis, *Prog Brain Res 58*, 465-478.
3. Changeux, J. P., Bon, F., Cartaud, J., Devillers-Thiery, A., Giraudat, J., Heidmann, T., Holton, B., Nghiem, H. O., Popot, J. L., Van Rapenbusch, R., and et al. (1983) Allosteric properties of the acetylcholine receptor protein from Torpedo marmorata, *Cold Spring Harb Symp Quant Biol 48 Pt 1*, 35-52.
4. Corringer, P. J., Le Novere, N., and Changeux, J. P. (2000) Nicotinic receptors at the amino acid level, *Annu Rev Pharmacol Toxicol 40*, 431-458.
5. Cassels, B. K., Bermudez, I., Dajas, F., Abin-Carriquiry, J. A., and Wonnacott, S. (2005) From ligand design to therapeutic efficacy: the challenge for nicotinic receptor research, *Drug Discov Today 10*, 1657-1665.
6. Ballivet, M., Patrick, J., Lee, J., and Heinemann, S. (1982) Molecular cloning of cDNA coding for the gamma subunit of Torpedo acetylcholine receptor, *Proc Natl Acad Sci U S A 79*, 4466-4470.
7. Giraudat, J., Devillers-Thiery, A., Auffray, C., Rougeon, F., and Changeux, J. P. (1982) Identification of a cDNA clone coding for the acetylcholine binding subunit of Torpedo marmorata acetylcholine receptor, *EMBO J 1*, 713-717.
8. Noda, M., Furutani, Y., Takahashi, H., Toyosato, M., Hirose, T., Inayama, S., Nakanishi, S., and Numa, S. (1982) Cloning and sequence analysis of cDNA for bovine adrenal preproenkephalin, *Nature 295*, 202-206.
9. Toyoshima, C., and Unwin, N. (1988) Ion channel of acetylcholine receptor reconstructed from images of postsynaptic membranes, *Nature 336*, 247-250.
10. Unwin, N., Toyoshima, C., and Kubalek, E. (1988) Arrangement of the acetylcholine receptor subunits in the resting and desensitized states, determined by cryoelectron microscopy of crystallized Torpedo postsynaptic membranes, *J Cell Biol 107*, 1123-1138.
11. Smit, A. B., Syed, N. I., Schaap, D., van Minnen, J., Klumperman, J., Kits, K. S., Lodder, H., van der Schors, R. C., van Elk, R., Sorgedrager, B., Brejc, K., Sixma, T. K., and Geraerts, W. P. (2001) A glia-derived acetylcholine-binding protein that modulates synaptic transmission, *Nature 411*, 261-268.
12. Unwin, N. (2005) Refined structure of the nicotinic acetylcholine receptor at 4A resolution, *J Mol Biol 346*, 967-989.
13. Grutter, T., and Changeux, J. P. (2001) Nicotinic receptors in wonderland, *Trends Biochem Sci 26*, 459-463.
14. Karlin, A. (2002) Emerging structure of the nicotinic acetylcholine receptors, *Nat Rev Neurosci 3*, 102-114.
15. Damle, V. N., and Karlin, A. (1980) Effects of agonists and antagonists on the reactivity of the binding site disulfide in acetylcholine receptor from Torpedo californica, *Biochemistry 19*, 3924-3932.
16. Czajkowski, C., Kaufmann, C., and Karlin, A. (1993) Negatively charged amino acid residues in the nicotinic receptor delta subunit that contribute to the binding of acetylcholine, *Proc Natl Acad Sci U S A 90*, 6285-6289.

17. Arias, H. R. (1997) Topology of ligand binding sites on the nicotinic acetylcholine receptor, *Brain Res Brain Res Rev 25*, 133-191.
18. Galzi, J. L., Bertrand, D., Devillers-Thiery, A., Revah, F., Bertrand, S., and Changeux, J. P. (1991) Functional significance of aromatic amino acids from three peptide loops of the alpha 7 neuronal nicotinic receptor site investigated by site-directed mutagenesis, *FEBS Lett 294*, 198-202.
19. Galzi, J. L., Revah, F., Bouet, F., Menez, A., Goeldner, M., Hirth, C., and Changeux, J. P. (1991) Allosteric transitions of the acetylcholine receptor probed at the amino acid level with a photolabile cholinergic ligand, *Proc Natl Acad Sci U S A 88*, 5051-5055.
20. Ma, J. C., and Dougherty, D. A. (1997) The Cationminus signpi Interaction, *Chem Rev 97*, 1303-1324.
21. Zhong, W., Gallivan, J. P., Zhang, Y., Li, L., Lester, H. A., and Dougherty, D. A. (1998) From ab initio quantum mechanics to molecular neurobiology: a cation-pi binding site in the nicotinic receptor, *Proc Natl Acad Sci U S A 95*, 12088-12093.
22. Brejc, K., van Dijk, W. J., Klaassen, R. V., Schuurmans, M., van Der Oost, J., Smit, A. B., and Sixma, T. K. (2001) Crystal structure of an ACh-binding protein reveals the ligand-binding domain of nicotinic receptors, *Nature 411*, 269-276.
23. Smit, A. B., Brejc, K., Syed, N., and Sixma, T. K. (2003) Structure and function of AChBP, homologue of the ligand-binding domain of the nicotinic acetylcholine receptor, *Ann N Y Acad Sci 998*, 81-92.
24. Dougherty, D. A., and Lester, H. A. (2001) Neurobiology. Snails, synapses and smokers, *Nature 411*, 252-253, 255.
25. Sullivan, D. A., and Cohen, J. B. (2000) Mapping the agonist binding site of the nicotinic acetylcholine receptor. Orientation requirements for activation by covalent agonist, *J Biol Chem 275*, 12651-12660.
26. Beene, D. L., Brandt, G. S., Zhong, W., Zacharias, N. M., Lester, H. A., and Dougherty, D. A. (2002) Cation-pi interactions in ligand recognition by serotonergic (5-HT3A) and nicotinic acetylcholine receptors: the anomalous binding properties of nicotine, *Biochemistry 41*, 10262-10269.
27. Le Novere, N., Grutter, T., and Changeux, J. P. (2002) Models of the extracellular domain of the nicotinic receptors and of agonist- and Ca2+-binding sites, *Proc Natl Acad Sci U S A 99*, 3210-3215.
28. Schapira, M., Abagyan, R., and Totrov, M. (2002) Structural model of nicotinic acetylcholine receptor isotypes bound to acetylcholine and nicotine, *BMC Struct Biol 2*, 1.
29. Celie, P. H., van Rossum-Fikkert, S. E., van Dijk, W. J., Brejc, K., Smit, A. B., and Sixma, T. K. (2004) Nicotine and carbamylcholine binding to nicotinic acetylcholine receptors as studied in AChBP crystal structures, *Neuron 41*, 907-914.
30. Gerzanich, V., Peng, X., Wang, F., Wells, G., Anand, R., Fletcher, S., and Lindstrom, J. (1995) Comparative pharmacology of epibatidine: a potent agonist for neuronal nicotinic acetylcholine receptors, *Mol Pharmacol 48*, 774-782.
31. Lindstrom, J., Anand, R., Peng, X., Gerzanich, V., Wang, F., and Li, Y. (1995) Neuronal nicotinic receptor subtypes, *Ann N Y Acad Sci 757*, 100-116.

32. Akk, G., and Auerbach, A. (1999) Activation of muscle nicotinic acetylcholine receptor channels by nicotinic and muscarinic agonists, *Br J Pharmacol 128*, 1467-1476.
33. Cashin, A. L., Petersson, E. J., Lester, H. A., and Dougherty, D. A. (2005) Using physical chemistry to differentiate nicotinic from cholinergic agonists at the nicotinic acetylcholine receptor, *J Am Chem Soc 127*, 350-356.
34. Mayo, S. L., Olafcon, B. D., and Goddard, W. A., III. (1990) *J. Phys. Chem. 94*, 8897-8909.
35. Springer-Verlag Lindahl, E. H., B.; van der Spoel, D. (2001) *J. Mol. Modeling 7*, 306-317.
36. Chipot, C. M., B.; Pearlman, D. A.; Kollman, P. A. (1996) *J. Am. Chem. Soc. 118*, 2998-3005.
37. Caldwell, J. W., Kollman, P. A. (1995) *J. Am. Chem. Soc. 117*, 4177-4178.
38. Changeux, J. P. (2009) Nicotinic receptors and nicotine addiction, *C R Biol 332*, 421-425.
39. Hogg, R. C., Raggenbass, M., and Bertrand, D. (2003) Nicotinic acetylcholine receptors: from structure to brain function, *Rev Physiol Biochem Pharmacol 147*, 1-46.
40. Millar, N. S., and Gotti, C. (2009) Diversity of vertebrate nicotinic acetylcholine receptors, *Neuropharmacology 56*, 237-246.
41. Rush, R., Kuryatov, A., Nelson, M. E., and Lindstrom, J. (2002) First and second transmembrane segments of alpha3, alpha4, beta2, and beta4 nicotinic acetylcholine receptor subunits influence the efficacy and potency of nicotine, *Mol Pharmacol 61*, 1416-1422.
42. Chavez-Noriega, L. E., Gillespie, A., Stauderman, K. A., Crona, J. H., Claeps, B. O., Elliott, K. J., Reid, R. T., Rao, T. S., Velicelebi, G., Harpold, M. M., Johnson, E. C., and Corey-Naeve, J. (2000) Characterization of the recombinant human neuronal nicotinic acetylcholine receptors alpha3beta2 and alpha4beta2 stably expressed in HEK293 cells, *Neuropharmacology 39*, 2543-2560.
43. Xiu, X., Puskar, N. L., Shanata, J. A., Lester, H. A., and Dougherty, D. A. (2009) Nicotine binding to brain receptors requires a strong cation-pi interaction, *Nature 458*, 534-537.
44. Filatov, G. N., and White, M. M. (1995) The role of conserved leucines in the M2 domain of the acetylcholine receptor in channel gating, *Mol Pharmacol 48*, 379-384.
45. Labarca, C., Nowak, M. W., Zhang, H., Tang, L., Deshpande, P., and Lester, H. A. (1995) Channel gating governed symmetrically by conserved leucine residues in the M2 domain of nicotinic receptors, *Nature 376*, 514-516.
46. Revah, F., Bertrand, D., Galzi, J. L., Devillers-Thiery, A., Mulle, C., Hussy, N., Bertrand, S., Ballivet, M., and Changeux, J. P. (1991) Mutations in the channel domain alter desensitization of a neuronal nicotinic receptor, *Nature 353*, 846-849.
47. Prince, R. J., and Sine, S. M. (1996) Molecular dissection of subunit interfaces in the acetylcholine receptor. Identification of residues that determine agonist selectivity, *J Biol Chem 271*, 25770-25777.

48. Gao, F., Bren, N., Burghardt, T. P., Hansen, S., Henchman, R. H., Taylor, P., McCammon, J. A., and Sine, S. M. (2005) Agonist-mediated conformational changes in acetylcholine-binding protein revealed by simulation and intrinsic tryptophan fluorescence, *J Biol Chem 280*, 8443-8451.
49. Henchman, R. H., Wang, H. L., Sine, S. M., Taylor, P., and McCammon, J. A. (2003) Asymmetric structural motions of the homomeric alpha7 nicotinic receptor ligand binding domain revealed by molecular dynamics simulation, *Biophys J 85*, 3007-3018.
50. Henchman, R. H., Wang, H. L., Sine, S. M., Taylor, P., and McCammon, J. A. (2005) Ligand-induced conformational change in the alpha7 nicotinic receptor ligand binding domain, *Biophys J 88*, 2564-2576.
51. Petersson, E. J. (2005) Investigations of ion channel structure and function. I. Studies of nicotine binding to the acetylcholine receptor. II. Development of tools for studying learning and memory with unnatural amino acids., in *Chemistry and Chemical Engineering*, Caltech, Pasadena.
52. Notredame, C., Higgins, D. G., and Heringa, J. (2000) T-Coffee: A novel method for fast and accurate multiple sequence alignment, *J Mol Biol 302*, 205-217.
53. Schrodinger, I. Prime, Portland, OR.
54. Guex, N., and Peitsch, M. C. (1997) SWISS-MODEL and the Swiss-PdbViewer: an environment for comparative protein modeling, *Electrophoresis 18*, 2714-2723.
55. van der Spoel, D., Lindahl, E., Hess, B., van Buuren, A.R., Apol, E., Meulenhoff, P.J., Tieleman, D.P., Sijbers, A.L.T.M., Feenstra, K.A., R., v. D., and Berendsen, H.J.C. (2004) Gromacs User Manual Version 3.2.
56. Schuettelkopf, A. W., and F., v. A. D. M., . (2004) *Acta Crystal D60*, 1355-1363.
57. Breneman, C. M. a. W., K.B. (1990) Determining atom-centered monopoles from molecular electrostatic potentials. The need for high sampling density in formamide conformational analysis., *J. Comp. Chem. 11*, 361-373.
58. Lee, W. Y., and Sine, S. M. (2004) Invariant aspartic Acid in muscle nicotinic receptor contributes selectively to the kinetics of agonist binding, *J Gen Physiol 124*, 555-567.
59. Cashin, A. L. (2006) Chemical scale investigations of drug-receptor interactions at the nicotinic acetylcholine receptor., in *Chemistry and Chemical Engineering*, California Institute of Technology, Pasadena, CA.
60. Torrice, M. M. (2008) Chemical-scale studies of the nicotinic and muscarinic acetylcholine receptors, in *Chemistry and Chemical Engineering*, California Institute of Technology, Pasadena, CA.
61. Gleitsman, K. R., Kedrowski, S. M., Lester, H. A., and Dougherty, D. A. (2008) An intersubunit hydrogen bond in the nicotinic acetylcholine receptor that contributes to channel gating, *J Biol Chem 283*, 35638-35643.
62. Cram, D. J. (1986) Preorganization-From Solvents to Spherands, *Angewandte Chemie-International Edition in English 25*, 1039-1057.
63. Nowak, M. W., Gallivan, J. P., Silverman, S. K., Labarca, C. G., Dougherty, D. A., and Lester, H. A. (1998) In vivo incorporation of unnatural amino acids into ion channels in Xenopus oocyte expression system, *Methods Enzymol 293*, 504-529.

64. England, P. M., Lester, H.A., and Dougherty, D.A. (1999) Incorporation of esters into proteins: improved synthesis of the hydroxyacyl tRNAs., *Tetrahedron Letters 40*, 6189-6192.
65. Saks, M. E., Sampson, J. R., Nowak, M. W., Kearney, P. C., Du, F., Abelson, J. N., Lester, H. A., and Dougherty, D. A. (1996) An engineered Tetrahymena tRNAGln for in vivo incorporation of unnatural amino acids into proteins by nonsense suppression, *J Biol Chem 271*, 23169-23175.
66. Kearney, P. C., Nowak, M. W., Zhong, W., Silverman, S. K., Lester, H. A., and Dougherty, D. A. (1996) Dose-response relations for unnatural amino acids at the agonist binding site of the nicotinic acetylcholine receptor: tests with novel side chains and with several agonists, *Mol Pharmacol 50*, 1401-1412.
67. Cashin, A. L., Torrice, M. M., McMenimen, K. A., Lester, H. A., and Dougherty, D. A. (2007) Chemical-scale studies on the role of a conserved aspartate in preorganizing the agonist binding site of the nicotinic acetylcholine receptor, *Biochemistry 46*, 630-639.